Temperature-independent giant dielectric response in transitional BaTiO3 thin films

*Arnoud S. Everhardt[1]†, Thibaud Denneulin[2,3], Anna Grünebohm[4], Yu-Tsun Shao[5], Petr Ondrejkovic[6], Silang Zhou[1], Neus Domingo[7], Gustau Catalan[7,8], Jiří Hlinka[6], Jian-Min Zuo[5], Sylvia Matzen[9], Beatriz Noheda[1,10]**

[1] Zernike Institute for Advanced Materials, University of Groningen, The Netherlands.
[2] CEMES-CNRS, F-31055 Toulouse Cedex 4, France.
[3] Ernst Ruska-Centre for Microscopy and Spectroscopy with Electrons (ER-C), Forschungszentrum Jülich, 52425 Jülich, Germany.
[4] ICAMS, Ruhr-Universität Bochum, 44801 Bochum, Germany.
[5] Department of Materials Science and Engineering, University of Illinois, Urbana, Illinois, USA.
[6] Institute of Physics of the Czech Academy of Sciences, Na Slovance 2, 18221 Praha 8, Czech Republic.
[7] Catalan Institute of Nanoscience and Nanotechnology (ICN2), CSIC, Barcelona Institute of Science and Technology Campus, Universitat Autonoma de Barcelona, Bellaterra, 08193 Barcelona, Spain.
[8] ICREA, 08193 Barcelona, Spain.
[9] Center for Nanoscience and Nanotechnology, UMR CNRS - Université Paris-Sud, Université Paris-Saclay, Avenue de la Vauve, 91120 Palaiseau, France.
[10] Groningen Cognitive Systems and Materials Centre (CogniGron), University of Groningen, The Netherlands.
† Presently at: Materials Science Division, Lawrence Berkeley National Laboratory, Berkeley, CA 94720, USA.

* E-mail: b.noheda@rug.nl

Keywords: ferroelectrics, transitional ferroelectrics, $BaTiO_3$, gradients, permittivity

Abstract

Ferroelectric materials exhibit the largest dielectric permittivities and piezoelectric responses in nature, making them invaluable in applications from supercapacitors or sensors to actuators or electromechanical transducers. The origin of this behavior is their proximity to phase transitions (PTs). However, the largest possible responses are most often not utilized due to the impracticality of using temperature as a control parameter and to operate at the PT. This has motivated the design of solid solutions with morphotropic phase boundaries (MPB) between different polar phases that are tuned by composition and that are weakly dependent of temperature. The flat energy landscapes close to these PTs give rise to polarization rotation under external stimuli, leading to intermediate (bridging or adaptive) phases, being responsible for the best piezoelectrics so far. But to achieve temperature-independent PT boundaries, complex chemistry or an intricate microstructure was so far required. Here we report such a temperature-independent bridging state in thin films of chemically simple $BaTiO_3$. A coexistence of tetragonal, orthorhombic and their bridging low-symmetry phases are shown to induce continuous vertical polarization rotation, recreating a smear in-transition state and leading to a giant temperature-independent dielectric response. Thus, we have engineered a ferroelectric state that is distinct from the MPB states but also displays a temperature-stable, highly responsive, in-transition state. We believe that other materials can be engineered in a similar way to form a wider class of ferroelectrics that we propose to coin as transitional ferroelectrics.

Phase transitions (PTs) are among the most interesting and ubiquitous phenomena in nature[1]. In materials science, they are responsible for the technological impact of ferromagnets, ferroelectrics[2], shape-memory alloys or memristors[3]. PTs are associated to desirably large, nonlinear changes in the order parameters (magnetization, polarization, resistance, etc.) and susceptibilities. However, they are often also associated to energy losses, resulting from the cost of nucleating one phase into the other.

Ferroelectrics are an interesting class of materials due to their spontaneous polarization and large responses to external stimuli (electric field or stress), which bestows them with the largest existing capacitances and electromechanical responses. Operating a ferroelectric near its transition temperature T_C[4–9] induces flattening of the energy potential and maximizes its dielectric and piezoelectric responses. However, the drawback is poor temperature stability. A way around this problem has been found by engineering phase boundaries between two polar phases via changes of a parameter that is robustly fixed during the lifetime of the device, such as composition. This approach requires careful tuning of the chemistry in order to obtain phase boundaries that are temperature-independent, that is parallel to the temperature axis in the temperature-composition phase diagram (known as morphotropic phase boundaries, MPB). This is the case of PZT or PMN-PT[5], the materials with the best performance. These are still used in most applications despite their lead content, as most alternatives lack the required temperature stability. More recently, compositional gradients have been utilized to achieve large dielectric responses[10], again requiring a careful control of the composition. Early pioneering work[11–15] has established that the origin of the large piezoelectric and dielectric responses around MPB's is the polarization rotation that takes place in low symmetry monoclinic or triclinic phases present at MPBs. In addition, because the MPB features and the low-symmetry phases are a result of the need for elastic matching of the different phases coexisting at the MPB[16], these exceptional properties do not always survive when the material is grown in thin film form, under demanding boundary conditions.

A similar phenomenon has been observed in $BaTiO_3$, at a so-called Thermotropic Phase Boundary[17], in between the tetragonal and orthorhombic phases, where a bridging low-symmetry phase can be found locally in a certain temperature regime around the phase transition. MPB-like features are also reported in $BiFeO_3$ thin films under strain, where two phases coexist and form a complex nano-domain structure with symmetry lowering, polar rotation and enhanced piezoelectric response[18] However, in these chemically simple compounds the temperature stability of the large responses has not been demonstrated.

In this paper we report a mechanism that leads to huge and temperature-independent dielectric responses and large piezoelectric responses in lead-free ferroelectric films of the classical ferroelectric $BaTiO_3$. In these films, the proximity to different stability minima renders evolving polar domain configurations within the same film, including intermediate bridging phases that support rotation of polarization. These materials cannot be considered ferroelectric crystals and we propose the term transitional ferroelectrics to emphasize their unique responses.

Effect of boundary conditions on the polar state and switching of $BaTiO_3$

$BaTiO_3$ thin films with thicknesses between 30 and 300 nm have been grown on $NdScO_3$ substrates with $SrRuO_3$ bottom (and optionally also top) electrodes by Pulsed Laser Deposition. Details can be found in the Methods section in Note S1 in the Supporting Information. Two different domain configurations had been reported to exist in these films close to room temperature[19]. One of the structures is the well-known a/c multi-domain phase, consisting of alternating in-plane (*a*-domain) and out-of-plane (*c*-domain) polarized regions, common in tetragonal thin films; the second structure was described as resembling the 90° in-plane domain configuration (a_1/a_2) with an additional weak out-of-plane component. However, the observed contrast in the Piezoelectric Force Microscopy (PFM) images was unusually weak for a strongly polar material, such as $BaTiO_3$, and the details of this complex domain structure and phase diagram are still under debate[19–23].

Dark-field Transmission Electron Microscopy (TEM) (Figure 1(a)) has been performed on these $BaTiO_3$ films to shed light on the details of the domain configurations throughout the film. Due to dynamical diffraction, the variations of contrast in dark-field TEM are related to variations of the ferroelectric polarization along the direction of the selected diffracted beam[24,25]. A strong dependence of the domain orientations both on thickness and on electrical boundary conditions is observed. Using quasi-symmetric and thick enough (above 10nm) electrodes, the films develop a 180° domain wall close to the center of the films, parallel to the film/electrode interfaces (hereafter referred to as "horizontal" direction), as evidenced in Figure 1(b) by the strong variation of contrast in the middle of the film and parallel to the interfaces. This wall takes place between c-like domains with opposite polarization direction induced by interfacial dipoles, in the top and bottom parts of the film, respectively, and it is similar to previous reports in ultra-thin $BaTiO_3$ films[26]. In Figure 1(c), the horizontal dark-field image shows periodic variations of contrast inclined at 45° with respect to the surface, which correspond to an a/c ferro-elastic/electric domain structure. The analysis of the strain fields (see Figure S1) has shown in-plane and out-of-plane strain variations at those 45° inclined domain walls. On the other hand, no additional strain was detected at the horizontal domain wall, confirming that the 180° horizontal domain wall is indeed purely ferroelectric. The overall polarization configuration in the film is shown schematically in Figure 1(d).

The polarization-voltage (hysteresis) loop measured along the out-of-plane direction of the film (Figure 2(a)) gives a saturation polarization of 25-30 $\mu C/cm^2$, similar to bulk $BaTiO_3$ (which is expected for this nearly zero-strain state[27]). However, the loop shows no remanence and the corresponding switching currents are wide and consist of two switching current peaks in each direction, instead of the one peak in each direction typically found for regular ferroelectric switching. This is consistent with the polarization switching of the two sublayers with up and down *c*-polarization, separated by the 180° domain wall observed in Figure 1. At zero field the two sublayers possess opposing c-polarizations, and under a field of +/- 0.1 V

(10 kV/cm, see also Figure S2), the polarization switches to a parallel configuration. During this process, the electromechanical coupling is strong with a measured piezoelectric coefficient with d_{33} = 70 pm/V. This d_{33} value is larger than that of typical $BaTiO_3$ epitaxial films[28] (as they are subjected to clamping[29]) and comparable to that of PZT or PMN-PT epitaxial films around the MPB[30,31] or $BaTiO_3$ bulk single crystals[32].

When the films are grown with asymmetric electrodes (a thin $SrRuO_3$ or platinum electrode), the horizontal 180° charged domain wall is moved away from the center of the film, close to the surface (Figure 1(e,f)). Concomitantly, the ferroelectric hysteresis loop also changes drastically (Figure 2(b)). The switching current loop now shows a single switching current peak with an internal bias of 0.15 V (20 kV/cm). In addition, a finite remanent polarization at zero field is now present, corresponding to the imbalance of up and down polarization induced by the asymmetric configuration (see also Figure S3). The piezoelectric loop displays the same internal bias as the ferroelectric hysteresis and shows increased d_{33} values of 100 pm/V at the bias, or switching, field, showcasing a highly asymmetric structure. Moreover, the films act as a 'strain diode'[33] as there is a significant difference between the piezoelectric constant at large positive (70 pm/V) and negative (20 pm/V) biases. In this case the effect is caused by the asymmetry of the electrodes, rather than by combining opposing ferroelectric and flexoelectric effects.

Temperature-independent giant dielectric permittivity

When the polarization is measured in the in-plane direction, a symmetric squared ferroelectric hysteresis loop similar to that of high-quality single crystals is obtained (Figure 3(a)). To achieve this state, a wake-up cycling had to be performed of 10^6 cycles (see inset) to remove pinched dipoles[34,35]. Such a wake-up cycling did not have to be performed along the out-of-plane direction, and moreover, such cycling did not have any effect on the properties at least up to 10^7 cycles. More details on these phenomena can be found in Figure S4,5. This loop reflects the high crystalline quality with a remanent polarization of ~12 $\mu C/cm^2$, in agreement

with the amount of *a*-polarization in these a/c structures[19]. Interestingly, these properties are only observed after field cycling, not uncommon for ferroelectric materials (see Figure S5). The in-plane dielectric permittivity and loss value (tan δ) (Figure 3(b)) are also typical for a ferroelectric material of excellent crystal quality, showing sharp switching signatures at the coercive field.

In contrast, the dielectric permittivity along the out-of-plane direction (which is independent of wake-up cycles) shows giant values, significantly larger than predicted for such films[20], with low losses, as observed in Figure 3(c) (see also Figure S6 for additional details). While the in-plane dielectric permittivity as function of temperature (after wake-up cycles performed at room temperature) (Figure 3(d)) shows a pronounced divergence (it reaches >25 000), as expected for ferroelectric crystals when approaching the ferroelectric-to-paraelectric phase transition (T_c~ 130 °C)[19] and, thus, denoting a large degree of ordering; the out-of-plane dielectric permittivity is remarkably stable under temperature variations and only significantly changes (decreases) above T_C. The value of this out-of-plane dielectric permittivity is comparable to that of $BaTiO_3$ single crystals at room temperature[36]. However, while in $BaTiO_3$ single crystals, the dielectric permittivity shows a strong temperature dependence, in the present case we show a giant temperature-independent dielectric permittivity, which – to the best of our knowledge – is larger than any of the temperature-independent dielectric permittivities reported for epitaxial thin films[8,10,37–39].

Vertical gradients

For a detailed understanding of the remarkable properties observed for these $BaTiO_3$ thin films along the out-of-plane direction, a closer look into the local structure of the films is needed. The films with dissimilar electrodes (Figure 4(a)) provide the opportunity to explore the local strain state across the film thickness unhindered by the horizontal 180° charged domain walls. A thick 320 nm $BaTiO_3$ film is used to increase the dimensions of the different phases that develop across the film thickness as strain relaxes. Figure 4(b) shows a bright-

field TEM image that displays 45° inclined a/c domains. However, the domain wall contrast disappears gradually, towards the bottom interface (Figure 4(c,d)). Local TEM polarization mapping, using scanning convergent beam electron diffraction (SCBED)[40–42], has been performed to understand the crystal symmetries involved (Figure 5(a)). Excellent agreement between the experiments (Figure 5(b,d,e)), and the simulated crystal symmetries (Figure 5(c,f)), evidences distinctly different regions across the films: at the top of the film, polarization vectors along [100]/[00-1] are consistent with tetragonal a/c domains (Figure 5(b,c)). At the bottom area of the film, the domains have orthorhombic symmetry, with polar vectors along [101]/[10-1] (Figure 5(e,f)). In the middle of the layer, there exists a complex transition region with reduced symmetry (Figure 5(d)), which cannot be reproduced in simulations, using either tetragonal or orthorhombic structure models. These monoclinc or triclinic (this distinction cannot be made in this 2D representation) lowered symmetry regions seen in the SCBED are not caused by averaging over multiple nanodomains[43], so resemble a true low-symmetry state. These observations are in agreement with the strain analysis of Figure 4(c,d). Here, dark-field electron holography[44] was used to measure the strain because it provides a large field of view (about 400×600 nm^2), which allows us to map the whole film. The map and strain profiles reveal strong strain gradients that increase from the bottom interface to the top surface. The rather homogeneous strain at the bottom of the film (Figure 4(c)) is consistent with [101]/[10-1] orthorhombic domains, which are indistinguishable from a strain point of view. Even though this film is significantly thicker than those used for the electrical measurements shown in Figure 2, similar multi-region mesostructures, though with lower resolution, are found for thinner films (Figure S7,8). The electrical results in this thicker film are similar to the thin films and indeed showcase a combination of this transition region (completely dominating the thin film) with a classical ferroelectric part, with some remanent polarization and a 2x temperature dependence (Figure S2). Thin films of $BaTiO_3$ under higher strain (on $GdScO_3$ substrates) have also revealed complex multiphase nanodomains[45].

To understand better the origin of the distinctly different phases found in these films, we have performed ab-*initio* effective Hamiltonian calculations as well as phase-field simulations (Figure S9-11). It is found that small changes in misfit strain (~0.01%) or energy (~2 meV/f.u.) are sufficient to stabilize either orthorhombic or tetragonal ferroelectric phases (see Figure S9-11). It is then, not unexpected to observe both types of symmetries within the same film. The need for them to coexist at the nanoscale brings intense stresses that deform the ferroelectric phases into lower symmetries and inhomogeneous structures.

Transitional ferroelectric enabled by polarization rotation

The $BaTiO_3$ films reported here have remarkable properties, with wide switching current peaks, no remanent polarization, huge dielectric permittivities and increased piezoelectric constants in the out-of-plane direction. Although some of these features may resemble relaxor materials, in this case, the $BaTiO_3$ films include none of the ingredients that are known to give rise to random fields or random bonds in relaxors. The in-plane measurement direction behaves like expected for a high-quality ferroelectric crystal, with a squared large remanent polarization hysteresis loops and a pronounced dielectric anomaly at the phase transition.
In the case of the asymmetric electrodes, along the out-of-plane direction, the strain and TEM analyses show a strain gradient, with low-symmetry phases bridging the expected tetragonal and orthorhombic phases, to provide a polarization rotation coupled to the strain gradient.
This low-symmetry transitional phase denote a flat energy landscape that enables continuous polarization rotation between the tetragonal and orthorhombic phase, which is independent of temperature. For the thin films, this transitional region spans the whole film, while for thicker films also traditional, non-transitional, regions exist which have their standard temperature-dependence near T_C (Figure S2(b)). The huge dielectric permittivity of >4000 originates from the easy rotation of the polarization even for small fields (Figure S6) due to the continuous polarization rotation mechanism. Similar materials with a polarization gradient but without

polarization rotation[10,46] or $BaTiO_3$ films without low-symmetry phases[27,47] do not show such temperature-independent response.

The quasi-symmetric electrode configuration shares these functional properties related to the low-symmetry phase, namely wide switching current peaks, increased piezoelectric d_{33} coefficient and huge temperature-independent dielectric permittivity, with the asymmetric case, as observed in Figure 2. The internal bias in the asymmetric configuration is created by uncompensated dipoles (as easily seen in Figure 5(a)) to create the asymmetric structure, leading to a strain diode, while in this quasi-symmetric configuration, the 180° domain wall in the center compensates those two sets of dipoles with two switching peaks to get an effective zero internal bias and more symmetric structure.

Some of the properties of this material resembles those of morphotropic phase boundaries (MPB's), in $PbZr_xTi_{1-x}O_3$ (PZT) and the ferroelectric relaxors solid solutions, as well as those of $BaTiO_3$ crystals at the thermotrophic phase boundary[17] or $BaTiO_3$ engineered nanodomains[48]. In addition, strain[18], stress[49] or electron beam radiation[48] can create multiple phases, multidomains and "ferroelectric-glass" states[48] that share some similar features with MPB systems, which have been shown to take advantage of displaying bridging phases at the boundary between two or more phases and to exhibit rotational degrees of freedom with an enhancement of the dielectric permittivity/piezoelectric response. However, not all these systems can be engineered such that the coexistence region and bridging phases are weakly dependent of temperature. The $BaTiO_3/NdScO_3$ system presents such intermediate, or transitional, state in a wide temperature range, similar to the MPB ferroelectrics. Nevertheless, microscopically, the material is clearly different since it cannot be considered a polycrystal but also not a single crystal, and it is not a relaxor but also not a homogeneous ferroelectric. The material presented here is closer to the compositionally graded ferroelectrics, but in this case, the grading is strain-mediated self-organized naturally during the material processing. Thus, we believe that it is appropriate to use a different name to refer to materials that exist in

an intermediate, or coexisting, state that is robust against temperature variations but that cannot be considered MPB materials. We propose to coin these materials as "transitional ferroelectrics".

Concluding, this work demonstrates that transitional states, enabled by polarization rotation gradients and engineered by utilizing materials with nearly-degenerate, differently- oriented polar phases, have properties that are distinct of those of single crystals, multi-domain crystals, ceramics or relaxor ferroelectrics. We show that, in $BaTiO_3$ thin films grown on $NdScO_3$ substrates with varying thicknesses of $SrRuO_3$ electrodes, these gradients facilitate an electrical-field induced gradual rotation of the polarization. While the in-plane direction shows standard ferroelectric behavior, the out-of-plane direction shows a flat energy landscape. It manages to achieve a giant dielectric permittivity with a large piezoelectric constant as would be characteristic of MPBs, while managing an exceptional temperature-stability without requiring demanding boundary conditions,. This combination of properties enables energy-efficient electromechanical functionalities and represents the dielectric equivalent of a magnetic permalloy - with high permittivity that is largely temperature-independent and with dielectric hard and easy axes. Similar mechanisms could be utilized in the design of other low power ferroelectrics, piezoelectrics, dielectrics or shape-memory alloys, as well as in efficient electro- and magneto-caloric cooling.

Acknowledgements

The authors are grateful to U. Bhaskar for preliminary piezoelectric measurements, to C. Magén for preliminary TEM measurements, to G. Agnus for developing oxides patterning processes and to N. Robin, P. Muralt and D. Damjanovic for useful discussions. A.S.E. and B.N. acknowledge financial support from the alumni organization of the University of Groningen, De Aduarderking (Ubbo Emmius Fonds), and from the Zernike Institute for Advanced Materials. T.D. acknowledges the European Metrology Research Programme (EMRP) Project IND54 397 Nanostrain and the European Union's Seventh Framework Programme (FP7/2007-2013)/ERC Grant Agreement No. 320832. T.D. thanks Knut Müller-Caspary for technical help with the STEM experiment. A.G. acknowledges funding by the Deutsche Forschungsgemeinschaft (SPP 1599 GR 4792/1-2 and GR 4792/2-1). Y.T.S. and J.M.Z. acknowledge the financial support by the DOE BES (Grant No. DEFG02-01ER45923).

Electron diffraction experiments were carried out at the Center for Microanalysis of Materials at the Frederick Seitz Materials Research Laboratory of University of Illinois at Urbana-Champaign. J.H. and P.O. were supported by the Operational Programme Research, Development and Education (financed by European Structural and Investment Funds and by the Czech Ministry of Education, Youth and Sports), Project No. SOLID21 - CZ.02.1.01/0.0/0.0/16_019/0000760). N.D. and G.C. acknowledge financial support by the Severo Ochoa Excellence programme.

References

[1] K.G. Wilson, Phys. Rev. B **4**, 3174 (1971).

[2] M.E. Lines and A.M. Glass, *Principles and Applications of Ferroelectrics and Related Materials* (Oxford University Press, Oxford, 1977).

[3] D.B. Strukov, G.S. Snider, D.R. Stewart, and R.S. Williams, Nature **453**, 80 (2008).

[4] F. Weyland, M. Acosta, J. Koruza, P. Breckner, J. Rödel, and N. Novak, Adv. Funct. Mater. **26**, 7326 (2016).

[5] S.H. Baek, J. Park, D.M. Kim, V.A. Aksyuk, R.R. Das, S.D. Bu, D.A. Felker, J. Lettieri, V. Vaithyanathan, S.S.N. Bharadwaja, N. Bassiri-Gharb, Y.B. Chen, H.P. Sun, C.M. Folkman, H.W. Jang, D.J. Kreft, S.K. Streiffer, R. Ramesh, X.Q. Pan, S. Trolier-McKinstry, D.G. Schlom, M.S. Rzchowski, R.H. Blick, and C.B. Eom, Science **334**, 958 (2011).

[6] Z. Luo, D. Zhang, Y. Liu, D. Zhou, Y. Yao, C. Liu, B. Dkhil, X. Ren, and X. Lou, Appl. Phys. Lett. **105**, 102904 (2014).

[7] W.J. Merz, Phys. Rev. **91**, 513 (1953).

[8] P. Zubko, N. Jecklin, N. Stucki, C. Lichtensteiger, G. Rispens, and J.-M. Triscone, Ferroelectrics **433**, 127 (2012).

[9] M. Acosta, N. Novak, V. Rojas, S. Patel, R. Vaish, J. Koruza, G.A. Rossetti, and J. Rödel, Appl. Phys. Rev. **4**, (2017).

[10] A.R. Damodaran, S. Pandya, Y. Qi, S.-L. Hsu, S. Liu, C. Nelson, A. Dasgupta, P. Ercius, C. Ophus, L.R. Dedon, J.C. Agar, H. Lu, J. Zhang, A.M. Minor, A.M. Rappe, and L.W. Martin, Nat. Commun. **8**, 14961 (2017).

[11] S.E. Park and T.R. Shrout, J. Appl. Phys. **82**, 1804 (1997).

[12] R. Guo, L.E. Cross, S.-E. Park, B. Noheda, D.E. Cox, and G. Shirane, Phys. Rev. Lett. **84**, 5423 (2000).

[13] L. Bellaiche, A. García, and D. Vanderbilt, Phys. Rev. Lett. **84**, 5427 (2000).

[14] H. Fu and R.E. Cohen, Nature **403**, 281 (2000).

[15] M. Davis, M. Budimir, D. Damjanovic, and N. Setter, J. Appl. Phys. **101**, 054112 (2007).

[16] Y.M. Jin, Y.U. Wang, A.G. Khachaturyan, J.F. Li, and D. Viehland, Phys. Rev. Lett. **91**, 197601 (2003).

[17] T.T.A. Lummen, Y. Gu, J. Wang, S. Lei, F. Xue, A. Kumar, A.T. Barnes, E. Barnes, S. Denev, A. Belianinov, M. Holt, A.N. Morozovska, S. V. Kalinin, L.-Q. Chen, and V. Gopalan, Nat. Commun. **5**, 3172 (2014).

[18] R.J. Zeches, M.D. Rossell, J.X. Zhang, A.J. Hatt, Q. He, C.-H.C.-H. Yang, A. Kumar, C.H. Wang, A. Melville, C. Adamo, G. S\ heng, Y.-H.Y.-H. Chu, J.F. Ihlefeld, R. Erni, C. Ederer, V. Gopalan, L.Q. Chen, D.G. Schlom, N.A. Spaldin, L.W. Martin, R. Ramesh, G. Sheng, Y.-H.Y.-H. Chu, J.F. Ihlefeld, R. Erni, C. Ederer, V. Gopalan, L.Q. Chen, D.G. Schlom, N.A. Spaldin, L.W. Martin, and R. Ramesh, Science **326**, 977 (2009).

[19] A.S. Everhardt, S. Matzen, N. Domingo, G. Catalan, and B. Noheda, Adv. Electron. Mater. **2**, 1500214 (2016).

[20] V.G. Koukhar, N.A. Pertsev, and R. Waser, Phys. Rev. B **64**, 214103 (2001).

[21] A. Grünebohm, M. Marathe, and C. Ederer, Appl. Phys. Lett. **107**, 102901 (2015).

[22] Y.L. Li and L.Q. Chen, Appl. Phys. Lett. **88**, 072905 (2006).

[23] S. Choudhury, Y.L. Li, L.Q. Chen, and Q.X. Jia, Appl. Phys. Lett. **92**, 2006 (2008).

[24] M. Tanaka, N. Kitamura, and G. Honjo, J. Phys. Soc. Japan **17**, 1197 (1962).

[25] T. Asada and Y. Koyama, Phys. Rev. B **70**, 104105 (2004).

[26] G. Sanchez-Santolino, J. Tornos, D. Hernandez-Martin, J.I. Beltran, C. Munuera, M. Cabero, A. Perez-Muñoz, J. Ricote, F. Mompean, M. Garcia-Hernandez, Z. Sefrioui, C. Leon, S.J. Pennycook, M.C. Muñoz, M. Varela, and J. Santamaria, Nat. Nanotechnol. **12**, 655 (2017).

[27] K.J. Choi, M. Biegalski, Y.L. Li, A. Sharan, J. Schubert, R. Uecker, P. Reiche, Y.B. Chen, X.Q. Pan, V. Gopalan, L.-Q. Chen, D.G. Schlom, and C.B. Eom, Science **306**, 1005 (2004).

[28] V. Thery, A. Bayart, J.-F. Blach, P. Roussel, and S. Saitzek, Appl. Surf. Sci. **351**, 480 (2015).

[29] R. Mahjoub, S.P. Alpay, and V. Nagarajan, Phys. Rev. Lett. **105**, 197601 (2010).

[30] A. Kholkin, M. Calzada, P. Ramos, J. Mendiola, and N. Setter, Appl. Phys. Lett. **69**, 3602 (1996).

[31] M. Boota, E.P. Houwman, M. Dekkers, M.D. Nguyen, K.H. Vergeer, G. Lanzara, G. Koster, and G. Rijnders, Sci. Technol. Adv. Mater. **17**, 45 (2016).

[32] S. Wada, S. Suzuki, T. Noma, T. Suzuki, M. Osada, M. Kakihana, S.-E. Park, L.E. Cross, and T.R. Shrout, Jpn. J. Appl. Phys. **38**, 5505 (1999).

[33] U.K. Bhaskar, N. Banerjee, A. Abdollahi, G. Rijnders, E. Solanas, and G. Catalan, Nanoscale **8**, 1293 (2016).

[34] M.I. Morozov and D. Damjanovic, J. Appl. Phys. **104**, 034107 (2008).

[35] K. Carl and K.H. Hardtl, Ferroelectrics **17**, 473 (1978).

[36] F. Jona and G. Shirane, *Ferroelectric Crystals* (Dover Publications, Inc., Mineola, 1993).

[37] J.H. Haeni, P. Irvin, W. Chang, R. Uecker, P. Reiche, Y.L. Li, S. Choudhury, W. Tian, M.E. Hawley, B. Craigo, A.K. Tagantsev, X.Q. Pan, S.K. Streiffer, L.Q. Chen, S.W. Kirchoefer, J. Levy, and D.G. Schlom, Nature **430**, 758 (2004).

[38] P. Gerber, C. Kügeler, U. Böttger, and R. Waser, J. Appl. Phys. **98**, 124101 (2005).

[39] E. Bousquet, M. Dawber, N. Stucki, C. Lichtensteiger, P. Hermet, S. Gariglio, J.M. Triscone, and P. Ghosez, Nature **452**, 732 (2008).

[40] K.H. Kim and J.M. Zuo, Ultramicroscopy **124**, 71 (2013).

[41] Y.T. Shao and J.M. Zuo, Acta Crystallogr. **73**, 708 (2017).

[42] Y.T. Shao and J.M. Zuo, Phys. Rev. Lett. **118**, 157601 (2017).

[43] K. Kim and J. Zuo, Acta Crystallogr. Sect. A **70**, 583 (2014).

[44] M. Hÿtch, F. Houdellier, F. Hüe, and E. Snoeck, Nature **453**, 1086 (2008).

[45] S. Kobayashi, K. Inoue, T. Kato, Y. Ikuhara, and T. Yamamoto, J. Appl. Phys. **123**, 064102

(2018).

[46] J. C. Agar, A. R. Damodaran, M. B. Okatan, J. Kacher, C. Gammer, R. K. Vasudevan, S. Pandya, R. V. K. Mangalam, G. A. Velarde, S. Jesse, N. Balke, A. M. Minor, S. V. Kalinin, and L. W. Martin, Nat. Mater. **15**, 549 (2016).

[47] A.R. Damodaran, E. Breckenfeld, Z. Chen, S. Lee, and L.W. Martin, Adv. Mater. **26**, 6341 (2014).

[48] R. Ahluwalia, N. Ng, A. Schilling, R.G.P. McQuaid, D.M. Evans, J.M. Gregg, D.J. Srolovitz, and J.F. Scott, Phys. Rev. Lett. **111**, 165702 (2013).

[49] M. Ahart, M. Somayazulu, R.E. Cohen, P. Ganesh, P. Dera, H.K. Mao, R.J. Hemley, Y. Ren, P. Liermann, and Z. Wu, Nature **451**, 545 (2008).

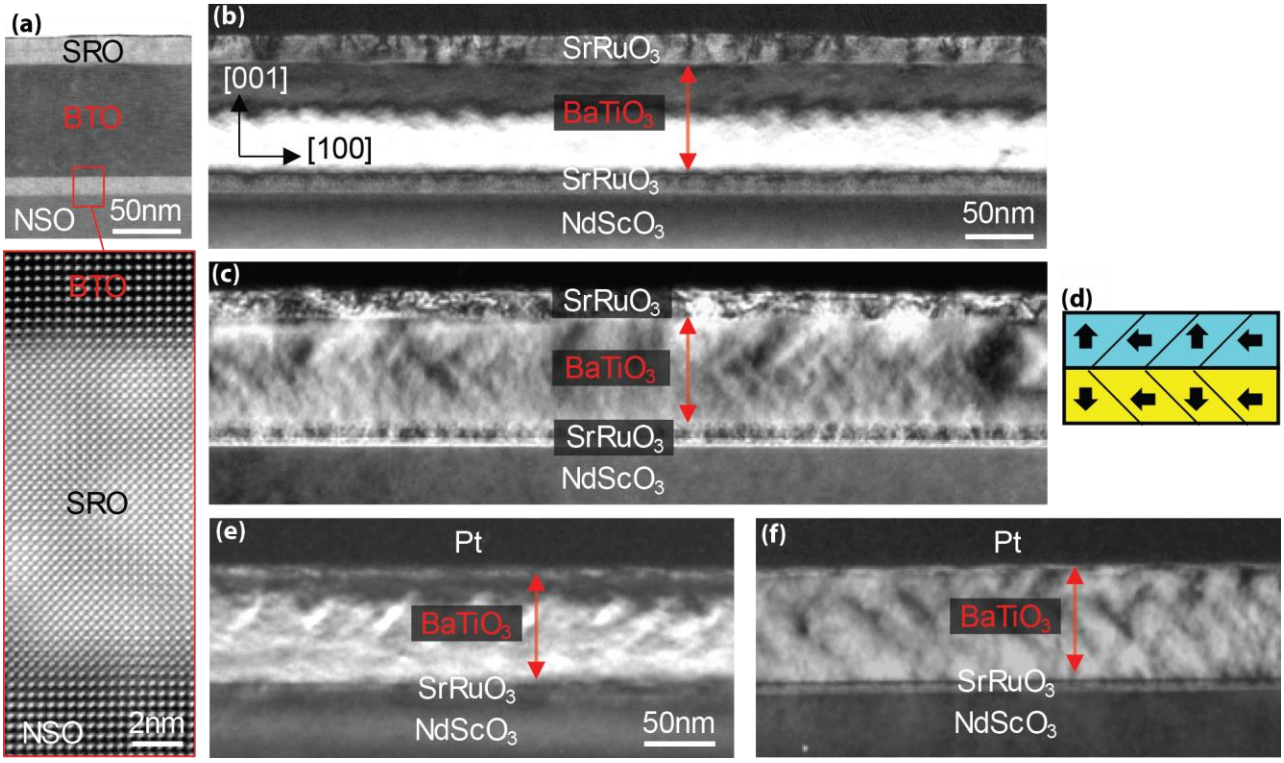

FIG 1. (a) High resolution STEM-HAADF image of an 80 nm thick $BaTiO_3$ film with a 12 nm $SrRuO_3$ bottom electrode and a 20 nm $SrRuO_3$ top electrode (the quasi-symmetric electrode configuration). The bottom image shows a magnified view of the $NdScO_3/SrRuO_3/BaTiO_3$ interfaces, which shows a defect-free epitaxial growth. (b) Vertical (002) dark-field TEM images of the previous sample that shows a strong variation of contrast in the middle of the film, attributed to a charged 180° domain wall. (c) Horizontal (200) dark-field image that

shows repeated variations of contrast at 45° to the interfaces, attributed to a/c (or 90°) twin domains. (d) Simplified schematics of the domain structure and polarization directions. The cyan region represents the averaged up-polarized, and the yellow the down-polarized state, as from the vertical dark-field. (e) Vertical (002) and (f) Horizontal (200) dark-field images of an 80 nm thick $BaTiO_3$ film with a (reduced) 6 nm $SrRuO_3$ bottom electrode and a 300 nm thick Pt top electrode (the asymmetric electrode configuration).

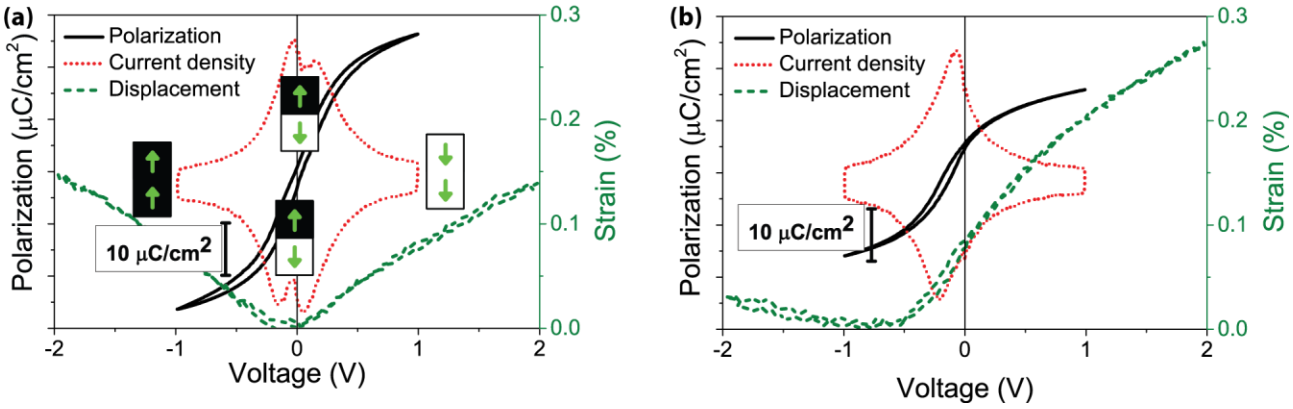

FIG 2. (a) An 80 nm $BaTiO_3$ thin film with quasi-symmetric 12 nm bottom and 20 nm $SrRuO_3$ top electrodes measured at room temperature for a 100 Hz electric field applied along the [001] out-of-plane direction. The insets show a sketch of the local averaged polarization above and below the original 180° horizontal domain wall. (b) $BaTiO_3$ film with asymmetric 6 nm $SrRuO_3$ bottom and 20 nm $SrRuO_3$ top electrodes. Note that the measurement technique can only measure differences in polarization.

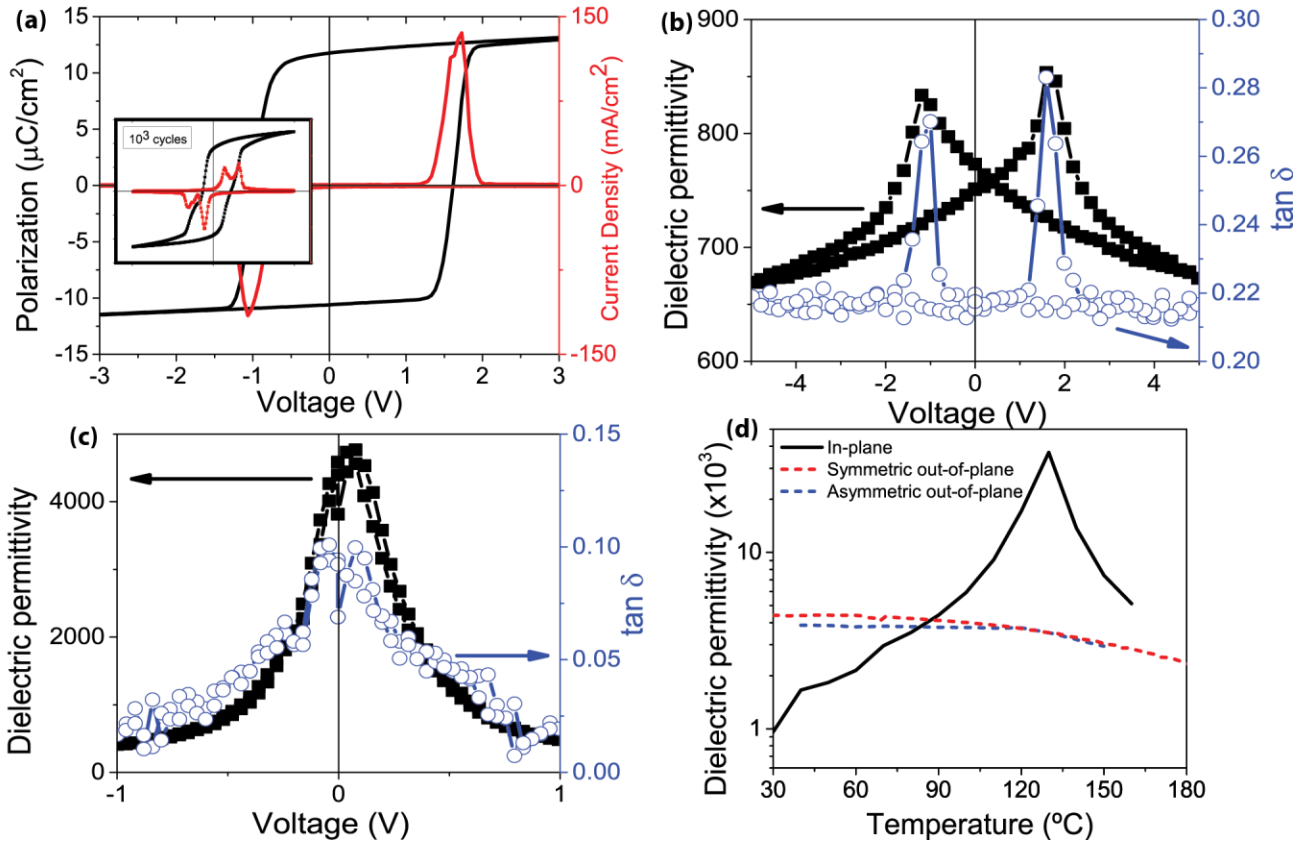

FIG 3. (a) Ferroelectric hysteresis loop for an 80 nm film at room temperature for a 100 Hz electric field along the [100] in-plane direction with 20 nm $SrRuO_3$ top electrodes and no bottom electrode with 5 µm spacing between the electrodes. Results obtained for this in-plane direction after 10^6 wake-up cycles, while the inset shows the results after 10^3 cycles. (b) In-plane dielectric permittivity and loss factor (tan δ) along [100] at a field frequency of 1 kHz and a small-signal voltage of 50 mV. (c) Out-of-plane (so along [001]) dielectric permittivity and loss factor (tan δ) at 1 kHz and a small-signal voltage of 50 mV using an 80 nm $BaTiO_3$ film with quasi-symmetric 12 nm bottom and 20 nm top $SrRuO_3$ electrodes. (d) Dielectric permittivity for 80 nm $BaTiO_3$ films as a function of temperature at a DC bias of 0 V at 1 kHz for the in-plane (black) and out-of-plane directions, red for *quasi*-symmetric electrodes and blue for asymmetric electrodes. The y-axis is in log(10) scale.

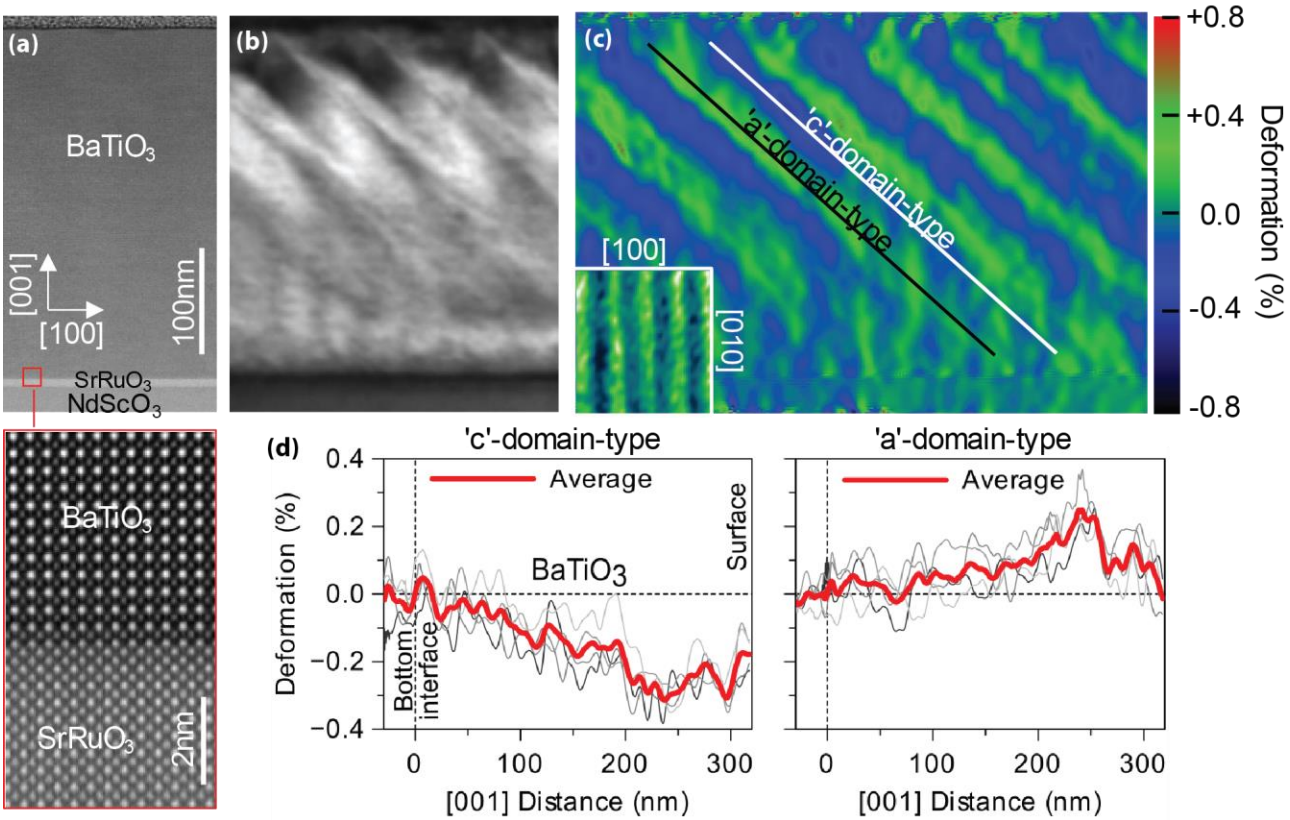

FIG 4. (a) Aberration-corrected STEM-HAADF (scanning transmission electron microscopy with a high angle annular dark-field detector) image of a 320 nm $BaTiO_3$ film grown on a $NdScO_3$ substrate with a 6 nm $SrRuO_3$ electrode and a thick Pt top electrode. (Top) low magnification image of the film and (bottom) high resolution image of the $SrRuO_3/BaTiO_3$ interface, which shows well-defined atomic columns and a defect-free crystal lattice. (b) Bright-field TEM image of the full film along the [010] direction showing some domain contrast. (c) In-plane deformation (E_{xx}) map obtained by dark-field electron holography, showing (101) domain walls in the $BaTiO_3$ film. E_{xx} is defined with respect to the substrate lattice parameter. The inset in the bottom left corner shows a Piezoelectric Force Microscopy (amplitude) image of the a/c domain structure at the sample surface (viewed along the [001] direction. (d) Deformation profiles extracted from the dashed regions in (c) running in the [101] direction and plotted as a function of the distance to the bottom electrode (along [001]), at both 'c'-domain-type (left) and 'a'-domain-type (right), as defined

by their polarization near the surface. The plots show the profiles of four distinct domains of each type (grey lines), as well as their average (red lines).

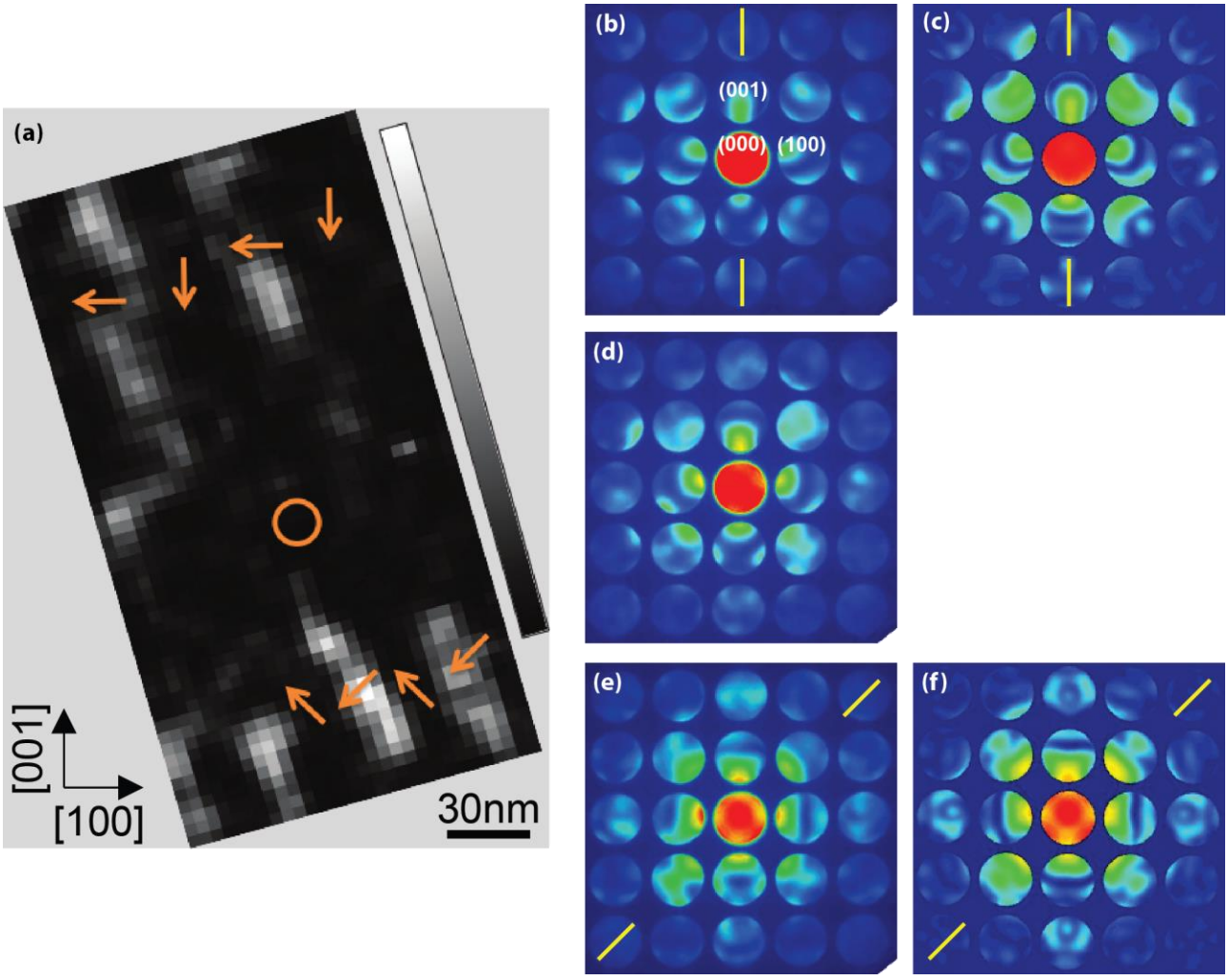

FIG 5. (a) A 320 nm $BaTiO_3$ film grown on a 6 nm $SrRuO_3$ electrode (not visible in the figure) and a thick Pt top electrode on a $NdScO_3$ substrate, measured along the [010] incidence at room temperature. Image reconstructed from a SCBED dataset where the intensity is determined by the polarity of the domains. The image was obtained by comparing the intensities of four <101> reflections. Orange arrows are a sketch of specific polarization vectors obtained from local CBED patterns. (b-f) CBED patterns measured or simulated for different regions at the film, showcasing good agreement between measurement and simulation. The orange lines indicate the mirror plane directions, corresponding to the polarization symmetry. (b) The polarizations at the top surface correspond to tetragonal [100]/[00-1] polarization directions. (c) Simulated CBED pattern for the tetragonal polarizations. (d) CBED pattern corresponding to the middle part of the film (this pattern comes from the orange circle in (a)), the polarization transition region. (e,f) Measured and simulated CBED patterns obtained in the bottom region of the film, corresponding to [101]/[10-1] polarization directions.